*J Mater Sci* (2022) 57:1186–1197

## Electronic materials

# Sol–gel preparation of Sn doped gallium oxide films for application in solar-blind ultraviolet photodetectors

Yana Li[1,3], Yuqiang Li[2,3], Yi Ji[1,3], Hong Wang[2,3,*], and Dingyong Zhong[1,3,*]

[1] *School of Physics, Sun Yat-Sen University, Guangzhou 510275, People's Republic of China*
[2] *School of Materials, Sun Yat-Sen University, Guangzhou 510275, People's Republic of China*
[3] *State Key Laboratory of Optoelectronic Materials and Technologies, Sun Yat-Sen University, Guangzhou 510275, People's Republic of China*

**Received:** 6 August 2021
**Accepted:** 27 October 2021
**Published online:**
3 January 2022

© The Author(s), under exclusive licence to Springer Science+Business Media, LLC, part of Springer Nature 2021

## ABSTRACT

$Ga_2O_3$ is considered as a candidate for the preparation of solar-blind photodetectors due to its large direct band gap. Developing low-cost preparation methods of high-quality $Ga_2O_3$ films is of importance for large-scale applications. In this work, we investigate the preparation of Sn doped β-$Ga_2O_3$ films by using simple and cheap sol–gel method under ambient condition. It is found that Sn doping induces a growth mode transformation from $(\bar{2}01)$ to $(\bar{3}11)$ oriented texture on the c-plane sapphire substrates. With an optimal Sn proportion, high-quality β-$Ga_2O_3$ films consisting of needle-like grains are observed. Compared with the undoped films, the Sn-doped films with needle-like grains obtained a low dark current of 0.76 nA, performed an on/off ratio as high as $\sim$ 6000, responsivity, $R$ of 164 mA/W and $D^*$ of $3.21 \times 10^{12}$ Jones at a bias voltage of 30 V in the configuration of metal–semiconductor–metal solar-blind deep ultraviolet detectors. This is the highest on/off ratio of $Ga_2O_3$ solar-blind photodetectors fabricated by sol–gel method reported up to now and has the potential to be applied in practical use.

Handling Editor: Kevin Jones.

Address correspondence to E-mail: wanghong3@mail.sysu.edu.cn; dyzhong@mail.sysu.edu.cn



https://doi.org/10.1007/s10853-021-06680-w

## GRAPHICAL ABSTRACT

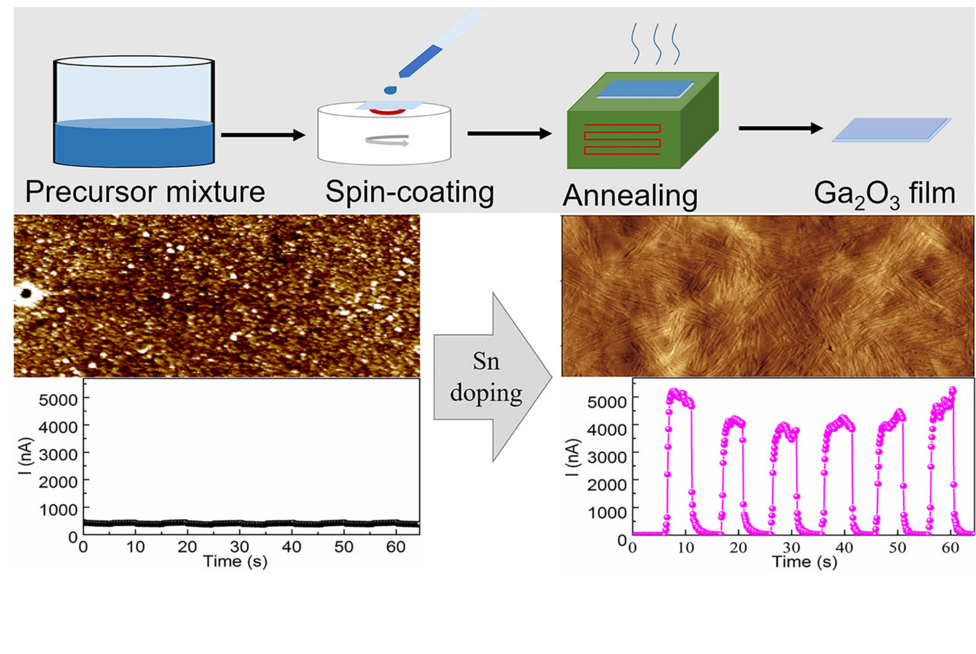


## Introduction

Deep ultraviolet (DUV) solar radiation with wavelength between 200 and 280 nm is hard to reach the earth's surface due to the strong absorption by stratospheric ozone [1, 2]. Solar-blind DUV detectors have the advantages of low background noise and high sensitivity, have been widely used in military and civil fields, e.g., military surveillance, missile launch detection, power grid security detection, medical imaging and biochemical detection [3–5]. Gallium oxide ($Ga_2O_3$) is a wide bandgap ($\sim$ 4.9 eV) semiconducting material with the light absorption band covering the range of solar-blind ultraviolet light [6, 7], which is considered to be an ideal material for DUV detectors.

To grow high-quality $Ga_2O_3$ thin films for fabricating DUV detectors with high performance, various thin film preparation techniques have been employed, including molecular beam epitaxy (MBE) [8–10], metal–organic chemical vapor deposition (MOCVD) [11, 12], pulsed laser deposition (PLD) [13, 14], magnetron sputtering [15, 16] and so on. However, these strategies often involve expensive vacuum equipment and complex operation steps. On the other hand, the sol–gel method is a relatively inexpensive manufacturing procedure, which has been previously applied in the perpetration of oxide semiconductor films such as ZnO, $TiO_2$ and ITO [17–20]. The sol–gel method was also applied to the preparation of $Ga_2O_3$ thin films. It was reported that the choice of precursor chemicals, solution environment and substrate surfaces is highly related to the structure and morphology of obtained $Ga_2O_3$ films [21–24]. In addition, researchers have also tried to change the crystalline phase, conductivity, light transmittance of obtained $Ga_2O_3$ films and corresponding response performance to light or oxygen by doping Mn, Cu, Zn, In, W and so on [25–28]. $Ga_2O_3$ films prepared by the sol–gel method have been used for fabricating DUV photodetectors. For example, Shen et al. fabricated β-$Ga_2O_3$ films with the sol–gel method and found that the film annealed at 700 °C had the best photoelectric performance along with fast response speed [29]. Furthermore, Yu et al. demonstrated the growth of α/β $Ga_2O_3$ thin films based on the sol–gel method and achieved high-performance solar-blind photodetectors by optimizing the annealing atmosphere and temperature [30].

However, in comparison with the $Ga_2O_3$ films prepared under vacuum conditions, currently the

films obtained by the sol–gel method usually exhibit poor crystalline quality and device performance. To improve the crystallinity, the films need to be annealed to a high temperature, which may lead to diffusion of atoms from the substrate into the gallium oxide film, resulting in the complicated film composition and suppressed photoelectric performance [31]. In this work, we synthesized Sn doped $Ga_2O_3$ films with improved crystalline quality through the sol–gel method with a post-annealing temperature of 700 °C. The Sn/Ga ratio can be easily adjusted by changing the solvent composition of the precursor solution. Moderate Sn doping changes the crystal growth mode on sapphire substrate and induces the formation of needle-like-grain β-$Ga_2O_3$ films with improved crystallinity. Compared with the undoped β-$Ga_2O_3$ films mainly composed of nanoparticles, the optimally doped films exhibit better detection performances for DUV device with a low dark current of 0.76 nA, reaching an on/off ratio as high as ~ 6000. This is the highest on/off ratio of $Ga_2O_3$ solar-blind photodetectors fabricated by the sol–gel method reported up to now and has the potential to be applied in practical use.

## Experimental section

### Materials

All the chemicals used in this work were purchased from commercial chemical reagent companies and were used directly without further purification treatment. 2-methoxyethanol ($C_3H_8O_2$, 99.8% purity) was purchased from Aladdin. Ethanolamine ($C_2H_7NO$, 99.5% purity) was purchased from Macklin. Isopropyl alcohol gallium (~ 99%) and isopropyl alcohol tin [~ 99% (metals basis), 10% W/V isopropanol solution] were purchased from Alfa Aesar.

### Preparation of $Ga_2O_3$ films and DUV photodetector

The preparation procedure of $Ga_2O_3$ films is illustrated in Fig. 1. Firstly, $C_3H_8O_2$ was mixed with $C_2H_7NO$ at room temperature and then heated to 60 °C for 1 h. Then, isopropyl alcohol gallium and isopropyl alcohol tin were added to the mixture in turn. The concentration of $C_2H_7NO$ was kept to be 0.5 mol/L, and the total amount of metal alkoxide was maintained at 1:1 to $C_2H_7NO$, where the Sn/Ga ratios are listed in Table 1. The samples are labeled as S1–S6 in the order of increasing Sn concentration. After that, the mixture was stirred at 60 °C for 1 h until it became clear and homogeneous, and then aged for 2 days at room temperature.

Secondly, the mixture was dropped onto a c-sapphire substrate (10 mm × 10 mm) and spin-coated at a rate of 3000 r/min for 20 s, followed by baking at 100 °C for 10 min and 300 °C for 20 min. The above-mentioned film preparation procedures were repeated 10 times to increase the film thickness. At last, the samples were annealed in a muffle oven at 700 °C for 2 h. During the experiments, the solution preparation and spin-coating procedures were carried out in a glove box, while the baking and annealing processes were carried out under ambient conditions with humidity of 45–50%.

The DUV photodetector electrodes (5 nm Ti / 60 nm Au) were deposited by physical vapor deposition through a shadow mask, in which 13 pairs of Ti / Au interdigital electrodes (100 μm width, 150 μm gap and 2800 μm length) were fabricated onto all the samples to form metal–semiconductor–metal (MSM) photodetectors.

### Characterization

All the as-prepared thin films were characterized by X-ray diffraction (XRD, Panalytical X'Pert Pro), UV − VIS spectrophotometer (UV 3600 Plus), atomic

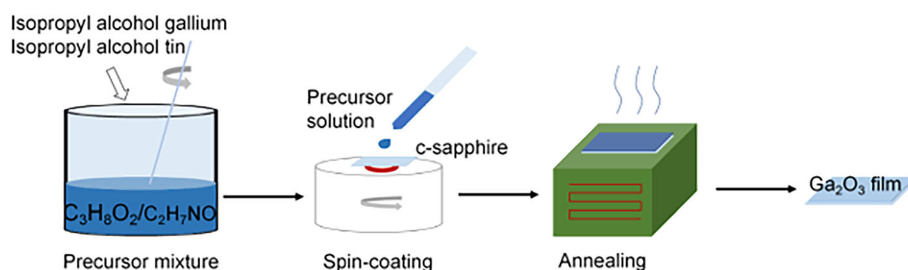


**Figure 1** Schematic illustration of preparation procedure of $Ga_2O_3$ films by sol–gel method.

**Table 1** Composition and characterization of β-$Ga_2O_3$ thin films

| Samples | S1 | S2 | S3 | S4 | S5 | S6 |
|---|---|---|---|---|---|---|
| Sn/Ga ratio (precursor) | 0 | 0.02 | 0.05 | 0.12 | 0.18 | 0.25 |
| Sn/Ga ratio (by XPS) | 0 | 0.018 | 0.042 | 0.078 | 0.14 | 0.22 |
| Sn/Ga ratio (by EDS) | 0 | 0.014 | 0.044 | 0.099 | 0.18 | 0.26 |
| RMS roughness (nm) | 0.58 | 1.42 | 2.28 | 6.86 | 6.32 | 6.92 |
| Bandgap values (eV) | 5.05 | 4.94 | 4.88 | 4.78 | 4.68 | 4.63 |

force microscope (AFM, OXFORD Cypher ES), scanning electron microscope (SEM, ZEISS AURIGA), energy-dispersive spectroscopy (EDS, ZEISS AURIGA) and X-ray photoelectron spectroscopy (XPS, Thermo-VG Scientific ESCALAB 250) to reveal their crystal structures, optical properties, surface morphologies, chemical bonding states and compositions. The current–voltage (I-V) properties and time-dependent photocurrents of the DUV devices were tested by a Source Meter Keysight 2902 to obtain data in dark and under illumination of a Hg lamp (254 nm UV) with power density of 0.3 $mW/cm^{-2}$ at a distance of ~ 1.5 cm from the lamb under ambient condition.

## Results and discussion

Figure 2 shows the XRD patterns of undoped $Ga_2O_3$ and Sn doped $Ga_2O_3$ thin films with various Sn contents. The diffraction peaks located at 20.5°, 37.5°and 41.7°are assigned to the (003), (110) and (006) planes of c-$Al_2O_3$ substrates [32]. For the undoped $Ga_2O_3$ film, obvious peaks at 18.9°, 38.4°

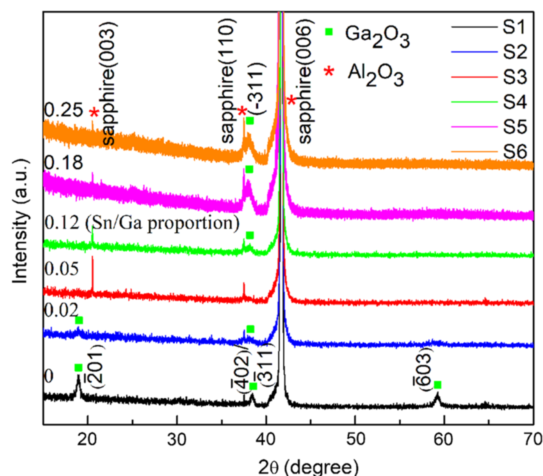


**Figure 2** XRD patterns of β-$Ga_2O_3$ thin films with various Sn doping contents.

and 59.2° were observed, which are attributed to the diffraction of $(\bar{2}01)$, $(\bar{4}02)$ and $(\bar{6}03)$ planes of β-$Ga_2O_3$, respectively [31]. With Sn doping into the films, the diffraction intensities of $(\bar{2}01)$, $(\bar{4}02)$ and $(\bar{6}03)$ planes decreased gradually and disappeared completely when the Sn/Ga proportion increased to 0.05. However, a new peak located at 38.1° indexed as $(\bar{3}11)$ of β-$Ga_2O_3$ was observed when the Sn/Ga proportion increased to 0.12. The intensity of the peak increased gradually with the Sn/Ga proportions increased from 0.12 to 0.25 (S4–S6 in Fig. 1). At the same time, the peak slightly shifted toward a smaller angle with increasing doping of Sn in β-$Ga_2O_3$, indicating the lattice expansion caused by the substitution of Ga ions (radius of 0.062 nm) by Sn ions (radius of 0.069 nm) [33, 34].

To reveal the morphology evolution of the samples with Sn doping, AFM characterization was performed on S1–S6 samples. As shown in Fig. 3a, the pure β-$Ga_2O_3$ film consists of tiny nanoparticles, exhibiting a smooth surface with a root mean square (RMS) roughness of 0.58 nm. With a 0.02 Sn/Ga proportion, the nanoparticles are in a smaller size with an increased roughness of 1.42 nm in comparison with those in the pure β-$Ga_2O_3$ film, as shown in Fig. 3b, which indicates a degrading crystallinity consistent with the XRD result. With further increasing the Sn/Ga proportion to 0.05, an amorphous film instead of crystalline nanoparticles with a roughness of 2.28 nm was observed, as shown in Fig. 3c. However, when the Sn/Ga proportion reaches 0.12, the film is mainly composed of needle-like grains as shown in Fig. 3d, displaying a rough surface with an RMS value of 6.86 nm. Compared with the nanoparticles, the needle-like grains have larger grain size and better atomic arrangement ordering in long range. Figure 3e shows the morphology of S5 with a Sn/Ga proportion of 0.18, where a film composed of needle-like grains with improved ordering of internal needles was obtained. The roughness of the film was calculated to be 6.32 nm,

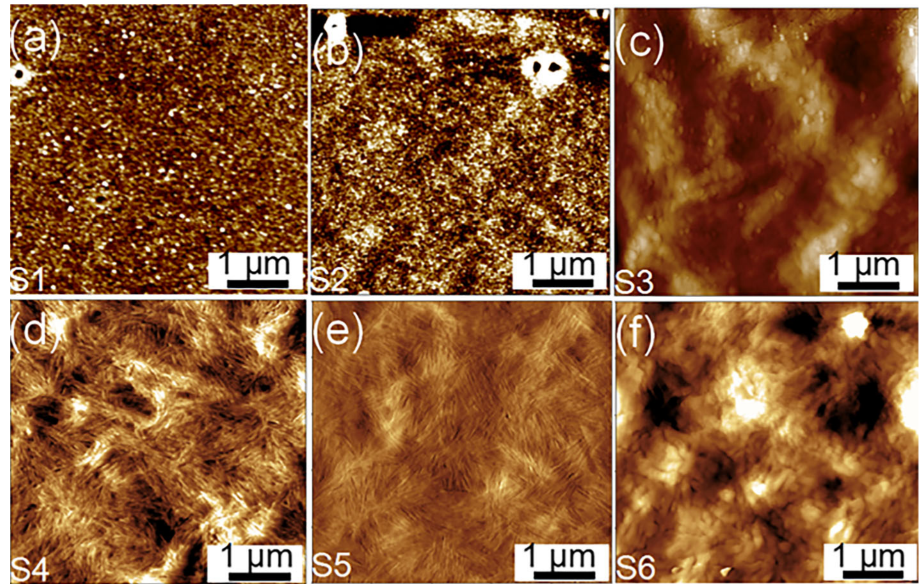


**Figure 3** **a**–**f** AFM topographies of β-$Ga_2O_3$ films (S1–S6) with various Sn/Ga proportions.

slightly smaller than that of S4. The morphology of S6 in Fig. 3f shows that the film is the roughest one and a new kind of short rod structure is formed when the Sn/Ga proportion increases to 0.25. The detailed RMS values of S1–S6 are listed in Table 1. To further confirm the change of the film morphology with Sn doping, SEM measurements were taken, as shown in Figure SI1a for S1 with a smooth surface. As a comparison, the needle-like grains of S5 were observed by SEM (Figure SI1b).

To reveal the chemical bonding states and composition of the films, XPS characterization of the

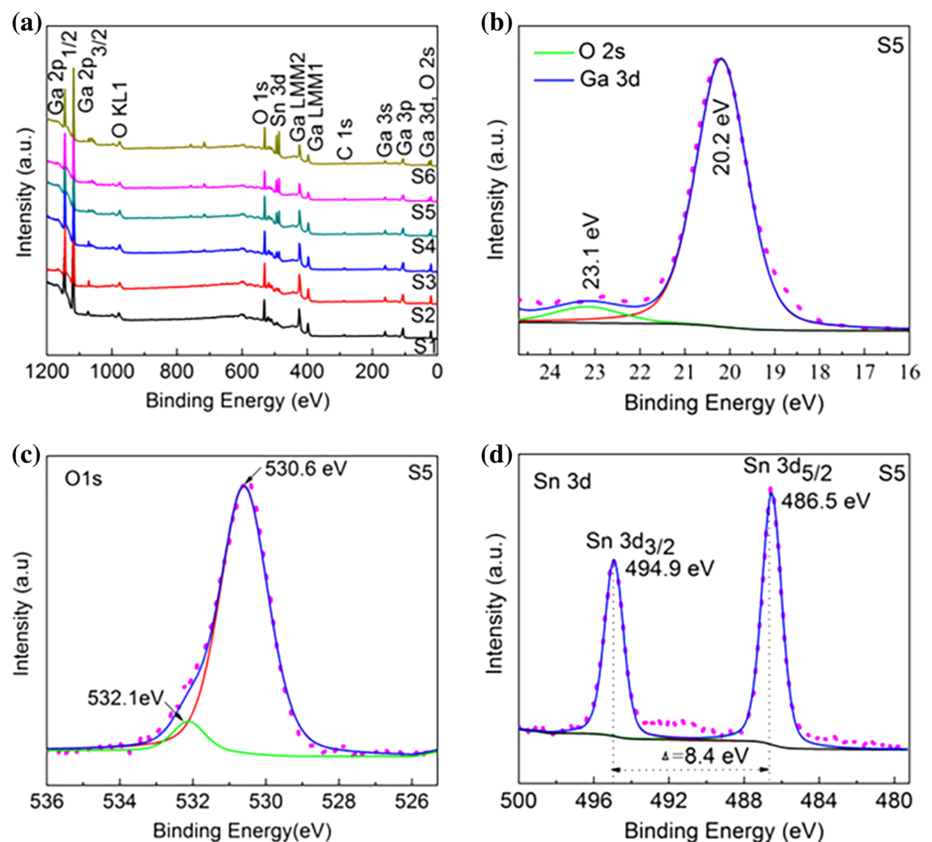


**Figure 4** **a** Typical XPS survey spectra of S1–S6. High-resolution core levels of **b** Ga 3d and O 2 s, **c** O1s and **d** Sn 3d spectra of sample S5.

samples was carried out, and the results are shown in Fig. 4. XPS survey spectra of S1–S6 are shown in Fig. 4a, where photoelectron spectra containing Ga (3d, 3p, 3 s, 2p and LMM), Sn (3d), O (2 s, 1 s, KLL and KVV) and C (1 s) peaks are detected [35, 36]. The C 1 s core levels fitted at 284.8 eV, 286.4 eV and 288.5 eV in Figure SI2 are related to the binding energy of C–C bond, C-O bond and C = O bond, respectively [37, 38]. All the binding energies are calibrated by the C–C bond at 284.8 eV from adventitious surface contamination [39]. Figure 4b shows the high-resolution spectrogram of the peak located at 20.2 eV, which is attributed to the $Ga^{3+}$ with Ga-O bond. Besides the peak, a weak O 2 s peak located at 23.1 eV is also observed [36, 40]. The core level of O 1 s in Fig. 4c can be fitted into two components. The main one located at 530.6 eV represents O-Ga bond for lattice $O^{2-}$ions, while the shoulder peak is related to the bonds originated from surface contamination, e.g., C-O and H–O bonds [35, 40]. Figure 4d shows the typical Sn 3d peaks at 486.5 and 494.9 eV with an energy difference of $\sim$ 8.4 eV, which are corresponding to the Sn $3d_{5/2}$ and $3d_{3/2}$ levels in the tetravalent $Sn^{4+}$ oxidation state, respectively [41, 42].

Additionally, the atomic ratio of Sn and Ga can be roughly estimated through the XPS spectra. The estimated Sn/Ga ratios obtained by XPS are shown in Table 1, and the obtained values are approximated to the ones of the initial quantity ratio of isopropyl alcohol gallium and isopropyl alcohol tin. Furthermore, energy-dispersive spectroscopy (EDS) was also employed to measure the Sn/Ga ratio of the samples as listed in Table 1, consistent with the results of XPS (see Figure SI3). Our work indicates that β-$Ga_2O_3$ thin films with various doping content of Sn can be obtained by directly adjusting the proportion of Sn in the precursor solution.

With the doping of Sn, the morphology of the β-$Ga_2O_3$ films switched from particle-like to needle-like. At the same time, Sn doping induces a growth mode transformation from $(\bar{2}01)$ to $(\bar{3}11)$ oriented texture on the c-plane sapphire substrates. We believe that the growth mode transformation is related to the lattice mismatch between epitaxial β-$Ga_2O_3$ film and the sapphire (0001) surface. Figure 5a shows the atomic arrangement schematic diagrams of the (0001) plane of sapphire substrate, where the unit cell is marked by dash lines. The right part shows the atom arrangement of $(\bar{2}01)$ plane of β-$Ga_2O_3$, where the lattice mismatch of β-$Ga_2O_3$[102] along $Al_2O_3$ $[11\bar{2}0]$ direction with the lattice ratio of 1:3, is estimated to be 3.2%, while the value of β-$Ga_2O_3$ [010] along $Al_2O_3$ $[\bar{1}100]$ with the lattice ratio of 8:3 is estimated to be -1.6%. Similarly, the lattice matching relationship between the $(\bar{3}11)$ plane of β-$Ga_2O_3$ and (0001) plane of $Al_2O_3$ is shown in Fig. 5b, where the lattice mismatches of β-$Ga_2O_3$ [121] along $Al_2O_3$ $[11\bar{2}0]$ direction with the lattice ratio of 1:3 and β-$Ga_2O_3$ $[01\bar{1}]$ along $Al_2O_3$ $[\bar{1}100]$ with the lattice ratio of 5:4 are estimated to be -4.3% and -0.68%, respectively. Obviously, β-$Ga_2O_3$ thin film without doping may be favorably and simultaneously grown with $(\bar{2}01)$-β-$Ga_2O_3$ on substrate as the XRD result of S1 because of the relatively small mismatch of $(\bar{2}01)$-β-$Ga_2O_3$/c-$Al_2O_3$, forming films consisting of nanoparticles [32, 43, 44]. With the doping of Sn ions, the lattice mismatch of β-$Ga_2O_3$ $(\bar{3}11)$ plane on sapphire would gradually decrease due to the larger radius of doped Sn ion (0.069 nm) compared with that of Ga ion (0.062 nm) [34], resulting in the formation of β-$Ga_2O_3$ films consisting of needle-like

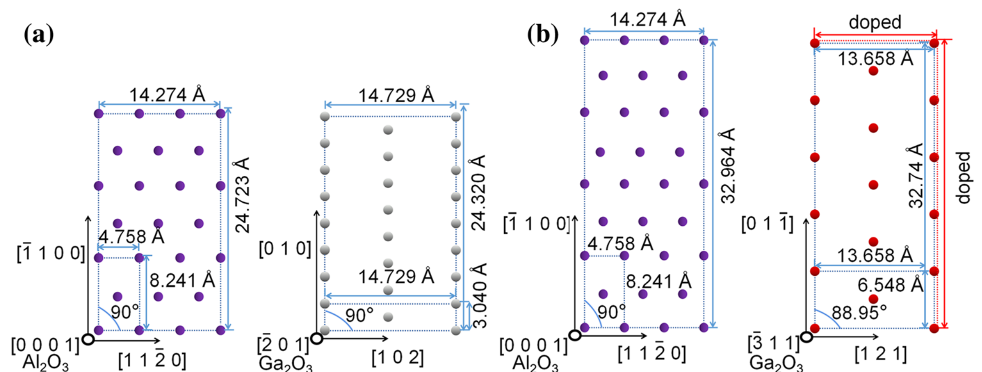


**Figure 5** Schematic description of lattice matching of **a** β-$Ga_2O_3$ $(\bar{2}01)$ and **b** β-$Ga_2O_3$ $(\bar{3}11)$ on $Al_2O_3$(001) substrate. The red dash lines in (b) show the extended lattice size after Sn doping.

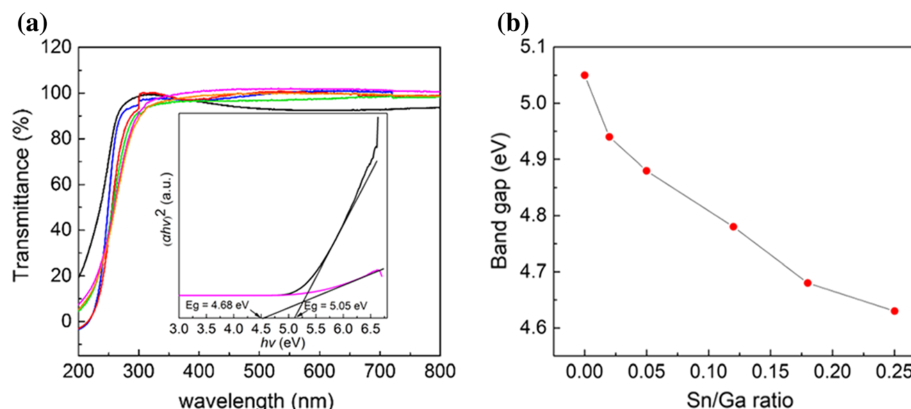


**Figure 6** **a** Transmittance spectra of $\beta$-$Ga_2O_3$ thin films of S1–S6. The inset shows the Tauc plots of S1 and S5. **b** Variation of bandgap with Sn/Ga ratio calculated from precursors for S1–S6 of $\beta$-$Ga_2O_3$ films.

grains when the Sn concentration increased to a certain value.

Figure 6a shows the transmission spectra of S1–S6. All the films exhibit high transmission of above 90% to UV–Vis light with wavelength above 300 nm. The spectrum of undoped $Ga_2O_3$ has a sharp intrinsic absorption edge located at about 250 nm. With the increasing Sn content, the absorption edges slightly shifted toward longer wavelength [34]. The optical band gap ($E_g$) can be calculated by the Tauc method according to the formula

$$\alpha h\nu = C\left(h\nu - E_g\right)^{1/2}$$

where $C$ is a constant, while $\alpha$ and $h\nu$ are the adsorption coefficient and incident photon energy, respectively [45, 46]. The inset of Fig. 6a shows the plots of $(\alpha h\nu)^2$ versus $h\nu$ of sample S1 and S5, and $E_g$ values are estimated by extrapolating the straight-line portion to the axis of photon energy [47, 48]. The bandgap of pure $\beta$-$Ga_2O_3$ was calculated to be 5.05 eV. Similarly, the bandgaps of doped samples can also be calculated (see Figure SI4). The plot of $E_g$ verse Sn/Ga proportion is shown in Fig. 6b, which decreases monotonously from 5.05 to 4.63 eV when the Sn/Ga proportion increased from 0 to 0.25.

To investigate the optoelectronic performance of those fabricated $\beta$-$Ga_2O_3$ films, MSM photodetectors with 13 pairs of Au interdigital electrodes (with electrode width of 100 μm and gap of 150 μm) were fabricated on the obtained $\beta$-$Ga_2O_3$ films by thermal evaporation under vacuum condition. A typical structure diagram of the DUV device is shown in Fig. 7a. Figure 7b shows the current–voltage (I-V) curves of S1, S3 and S5 with bias voltage varying from 0 to 30 V, where the dark currents $I_{dark}$ are measured to be 263, 131 and 0.76 nA, respectively. Note that the $I_{dark}$ of pure $\beta$-$Ga_2O_3$ fabricated by our method is much larger than those prepared by epitaxial growth methods in vacuum, as well as those prepared by the sol–gel method by employing gallium nitrate hydrate as precursor. We speculate that the large $I_{dark}$ is attributed to the poor crystallization quality due to the relatively low annealing temperature (700 °C). The dark currents decrease with the doping of Sn (sample S3 and S5) due to the crystalline and surface morphology change [49]. The samples were illuminated by a mercury lamp with the power density of 0.3 $mW/cm^{-2}$ at a distance of 1.5 cm to test the photocurrent $I_{light}$. Different $I_{light}/I_{dark}$ ratios can be obtained at the same bias voltage. Sample S5 obtains the largest value of 6039 at a bias voltage of 30 V, while the corresponding values of S1 and S3 are 1.34 and 2.08, respectively. All the $I_{dark}$, $I_{light}$ and on/off ratios of the samples from S1 to S6 are summarized in Table 2 at a bias voltage of 30 V. Obviously, the improved crystallinity of the film leads to a large photoelectric response owing to the low density of defect traps. In this case, less charge carrier might be captured during the charge transport process.

Furthermore, the responsivities $R$ of the films at a bias voltage of 30 V were calculated by the formula:

$$R = \left(I_{light} - I_{dark}\right)/(P_\lambda \times S)$$

where $P_\lambda$ is the irradiation power density, and $S$ is the effective illuminated area [50]. The $R$ of the samples of S1, S3 and S5 were calculated to be 3.19, 5.09 and 164 mA/W, respectively.

Detectivity ($D^*$) was calculated to evaluate the detection ability of those devices to DUV through equation

$$D* = A^{1/2}R/(4k_0T/R_{dark} + 2qI_{dark})^{1/2}$$

where $A$ is the active area, $R$ is the responsivity, $k_0$ is the Boltzmann constant, $T$ is the temperature, $R_{dark}$ is

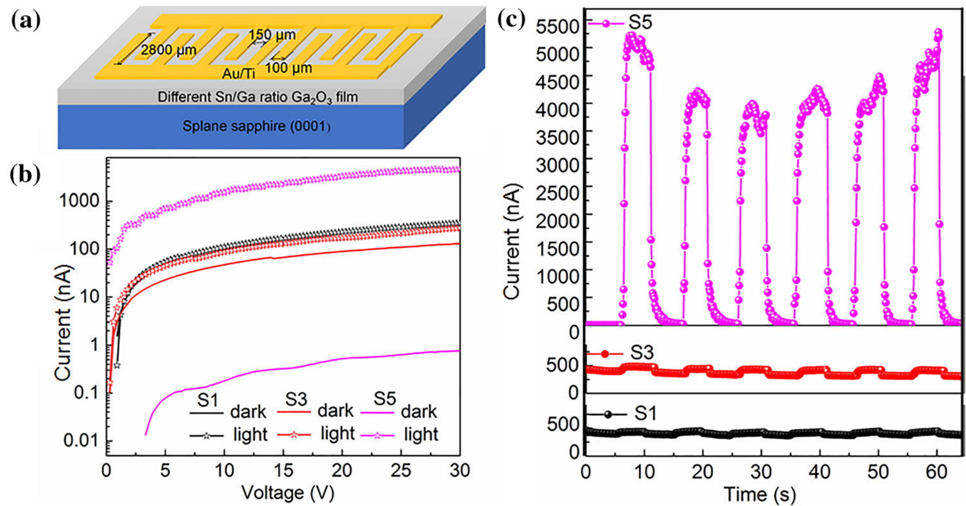


**Figure 7** Photoelectric properties of S1, S3 and S5 MSM photodetectors: **a** Schematic illustration of the photodetector; **b** I − V characteristics of the samples; **c** time-dependent photoresponse under UV light illumination.

**Table 2** The characteristic parameters of DUV photodetectors based on β-$Ga_2O_3$ films with the ratio of Sn/Ga varied from 0 to 0.25

| Sample | $I_{dark}$ (nA) | $I_{light}$ (nA) | $I_{light}/I_{dark}$ | $R$ (mA/W) | $D^*$ (Jones) | $t_r$ (s) | $t_d$ (s) |
|---|---|---|---|---|---|---|---|
| S1 | 263 | 352 | 1.34 | 3.19 | $3.35 \times 10^9$ | 0.41 | 0.15 |
| S2 | 190 | 226 | 1.19 | 1.29 | $1.59 \times 10^9$ | 0.27 | 0.13 |
| S3 | 131 | 273 | 2.08 | 5.09 | $7.57 \times 10^9$ | 0.62 | 0.10 |
| S4 | 7.41 | 400 | 54.0 | 14.1 | $8.80 \times 10^{10}$ | 0.27 | 0.23 |
| S5 | 0.76 | 4590 | 6039 | 164 | $3.21 \times 10^{12}$ | 0.42 | 0.20 |
| S6 | 6.27 | 2580 | 411 | 92.2 | $6.27 \times 10^{11}$ | 0.53 | 0.22 |

the equivalent resistance, $q$ is the elementary charge and $I_{dark}$ is the dark current [51, 52]. The calculated $D^*$ values are listed in Table 2 and the highest value is $3.21 \times 10^{12}$ Jones from S5. Our result indicates that, by adjusting the Sn doping content to an optimal value, the performance of the photodetectors can be significantly improved.

Figure 7c shows typical time-dependent photoelectric response curves of S1, S3 and S5 by shining the sample under a mercury lamp with the light source switched on and off every 5 s. The dark current of all the samples can go back to a low value after the light was turned off, showing fine repeatability of those obtained devices.

The response speed directly reflects the response-ability of a photoelectric device to optical signal when shown by UV light or cut off the light. The response rise time ($t_r$) is defined as the time required for the $I_{light}$ of a photodetector to increase from 10 to 90% of the peak value when the light is turned on [53], while the decay time ($t_d$) is the time for a photodetector to reduce $I_{light}$ from 90 to 10% when the light is turned off. Figure 8a–c shows the single-cycle response curves of the DUV devices based on S1, S3 and S5, and the extracted $t_r$ and $t_d$ are estimated to be 0.41 s / 0.15 s, 0.62 s / 0.10 s and 0.42 s / 0.20 s, respectively. The response speed is highly related to the generation and recombination of photogenerated carriers, which is dependent on the crystalline quality of the film as well as the transmission of carriers through the electrodes. The $t_r$ retains a similar value of the three samples, while the $t_d$ increases with the doping of Sn due to the introduced $Sn^{4+}$ in the lattice structure of β-$Ga_2O_3$ acted as traps to delay the release of photogenerated carriers. Similarly, the sample of S2, S4 and S6 exhibits similar behavior as shown in Figure SI5.

Table 2 summarizes the performance of typical MSM photodetectors based on β-$Ga_2O_3$ thin films with and without Sn doping. One can find that slight doping of Sn has little effect on the performance of the devices. But when the proportion of Sn in the precursor reaches 0.12, the growth mode transformation of β-$Ga_2O_3$ induced the great improvement in device performance, including the reduced dark current $I_{dark}$ and improved $I_{light}/I_{dark}$ ratio, $R$ and $D^*$.

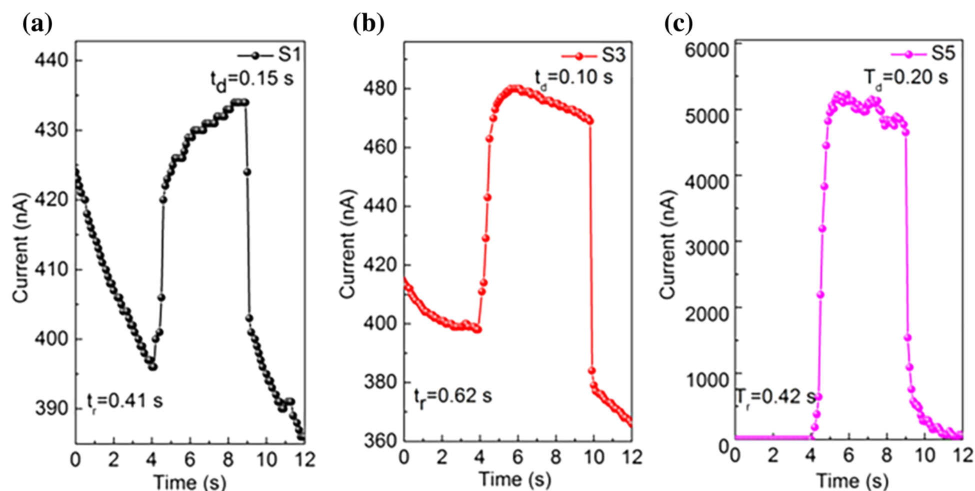


**Figure 8** Single-cycle response curves of photodetectors based on **a** S1, **b** S3 and **c** S5.

However, excessive Sn doping (S6) might lead to the decline of gallium oxide crystalline quality, resulted in deteriorating device performance. Although the photodetector performance is not as good as the ones fabricated under vacuum conditions, it is much improved of the sample with 0.18 Sn doped β-$Ga_2O_3$ films compared with those without Sn doping prepared by sol–gel method reported in the literature [29, 30]. Our work develops a low-cost method to prepare β-$Ga_2O_3$ thin films for solar-blind detectors under ambient condition.

## Conclusions

In summary, we have prepared β-$Ga_2O_3$ films by the sol–gel method with various Sn doping contents. A novel needle-like grain structure has been obtained in the doped films deposited on c-plane sapphire substrates. The β-$Ga_2O_3$ films consisting of needle-like grains show better crystallinity than that of pure β-$Ga_2O_3$ films. The growth mode transformation is attributed to the better lattice matching of β-$Ga_2O_3$ ($\bar{3}11$) plane to c-sapphire (0001) than that of β-$Ga_2O_3$ ($\bar{2}01$) due to the increased ion diameter of doped $Sn^{4+}$. The optimally doped films with needle-like grains exhibit highly improved solar-blind deep ultraviolet detection performance, e.g., dark current of 0.76 nA, on/off ratio as high as ~ 6000, responsivity $R$ of 164 mA/W and $D^*$ of 3.21 × $10^{12}$ Jones at a bias voltage of 30 V in the metal–semiconductor–metal configuration. Our work paves the way for the preparation of solar blind DUV photodetectors with low cost and high performance under ambient condition.

## Acknowledgements

This work was supported by NSFC (Grant No. 11974431 and 21661132006), Shenzhen Science and Technology Innovation Commission (STIC) (JCYJ20190807155411277) and the Fundamental Research Funds for the Central Universities, Sun Yat-sen University.

## Declarations

**Conflict of interest** The authors declare that they have no known competing financial interests or personal relationships that could have appeared to influence the work reported in this paper.

**Supplementary Information:** The online version contains supplementary material available at https://doi.org/10.1007/s10853-021-06680-w.

## References

[1] Xie C, Lu X, Liang Y et al (2021) Patterned growth of β-$Ga_2O_3$ thin films for solar-blind deep-ultraviolet photodetectors array and optical imaging application. J Mater Sci Technol 72:189–196. https://doi.org/10.1016/j.jmst.2020.09.015

[2] Xu J, Zheng W, Huang F (2019) Gallium oxide solar-blind ultraviolet photodetectors: a review. J Mater Chem C 7:8753–8770. https://doi.org/10.1039/c9tc02055a

[3] Kong W, Wu G, Wang K et al (2016) Graphene-β-$Ga_2O_3$ heterojunction for highly sensitive deep UV photodetector application. Adv Mater 28:10725–10731. https://doi.org/10.1002/adma.201604049

[4] Li L, Lee PS, Yan C et al (2010) Ultrahigh-performance solar-blind photodetectors based on individual single-crystalline $In_2Ge_2O_7$ nanobelts. Adv Mater 22:5145–5149. https://doi.org/10.1002/adma.201002608

[5] Zhuo Y, Chen Z, Tu W, Ma X, Pei Y, Wang G (2017) β-$Ga_2O_3$ versus ε-$Ga_2O_3$: Control of the crystal phase composition of gallium oxide thin film prepared by metal-organic chemical vapor deposition. Appl Surf Sci 420:802–807. https://doi.org/10.1016/j.apsusc.2017.05.241

[6] Pearton SJ, Yang J, Cary PH et al (2018) A review of $Ga_2O_3$ materials, processing, and devices. Appl Phys Rev 5:011301. https://doi.org/10.1063/1.5006941

[7] Zhao B, Wang F, Chen H et al (2017) An ultrahigh responsivity (9.7 mA $W^{-1}$) self-powered solar-blind photodetector based on individual ZnO-$Ga_2O_3$ heterostructures. Adv Funct Mater 27: 1700264. https://doi.org/10.1002/adfm.201700264

[8] Ai M, Guo D, Qu Y et al (2017) Fast-response solar-blind ultraviolet photodetector with a graphene/β-$Ga_2O_3$/graphene hybrid structure. J Alloys Compd 692:634–638. https://doi.org/10.1016/j.jallcom.2016.09.087

[9] Wu Z, Jiao L, Wang X et al (2017) A self-powered deep-ultraviolet photodetector based on an epitaxial $Ga_2O_3$/Ga:ZnO Heterojunction. J Mater Chem C 5:8688–8693. https://doi.org/10.1039/c7tc01741c

[10] Guo D, Wu Z, Li P et al (2014) Fabrication of β-$Ga_2O_3$ thin films and solar-blind photodetectors by laser MBE technology. Opt Mater Express 4:1067–1076. https://doi.org/10.1364/ome.4.001067

[11] Li Y, Zhang D, Lin R, Zhang Z, Zheng W, Huang F (2019) Graphene interdigital electrodes for improving sensitivity in a $Ga_2O_3$: Zn deep-ultraviolet photoconductive detector. ACS Appl Mat Interfaces 11:1013–1020. https://doi.org/10.1021/acsami.8b14380

[12] Ravadgar P, Horng RH, Yao SD et al (2013) Effects of crystallinity and point defects on optoelectronic applications of β-$Ga_2O_3$ epilayers. Opt Express 21:24599–24610. https://doi.org/10.1364/OE.21.024599

[13] Li KH, Alfaraj N, Kang CH et al (2019) Deep-ultraviolet photodetection using single-crystallineβ-$Ga_2O_3$/NiO heterojunctions. ACS Appl Mater Interfaces 11:35095. https://doi.org/10.1021/acsami.9b10626

[14] Vu TKO, Lee DU, Kim EK (2020) The enhancement mechanism of photo-response depending on oxygen pressure for $Ga_2O_3$ photo detectors. Nanotech 31:245201. https://doi.org/10.1088/1361-6528/ab76f5

[15] Li Z, An Z, Xu Y et al (2019) Improving the production of high-performance solar-blind β-$Ga_2O_3$ photodetectors by controlling the growth pressure. J Mater Sci 54:10335–10345. https://doi.org/10.1007/s10853-019-03628-z

[16] Arora K, Goel N, Kumar M, Kumar M (2018) Ultrahigh performance of self-powered β-$Ga_2O_3$ thin film solar-blind photodetector grown on cost-effective Si substrate using high-temperature seed layer. ACS Photonics 5:2391–2401. https://doi.org/10.1021/acsphotonics.8b00174

[17] Li Z, Ren D (2007) Fabrication and structure characterization of IT0 transparent conducting film by sol-gel technique. Trans Nonferrous Met Soc China 17:665–668. https://doi.org/10.1016/s1003-6326(07)60153-8

[18] Wen T, Gao J, Shen J, Zhou Z (2001) Preparation and characterization of $TiO_2$ thin films by the sol-gel process. J Mater Sci 36:5923–5926. https://doi.org/10.1023/A:1012989012840

[19] Kim YH, Heo JS, Kim TH et al (2012) Flexible metal-oxide devices made by room-temperature photochemical activation of sol-gel films. Nature 489:128–132. https://doi.org/10.1038/nature11434

[20] Pakma O, Serin N, Serin T (2009) The effect of repeated annealing temperature on the structural, optical, and electrical properties of $TiO_2$ thin films prepared By dip-coating sol-gel method. J Mater Sci 44:401–407. https://doi.org/10.1007/s10853-008-3145-5

[21] Chen D, Xu Y, An Z, Li Z et al (2019) Thin-film transistors based on wide bandgap $Ga_2O_3$ films grown by aqueous-solution spin-coating method. Micro & Nano Letters 14: 1052–1055. https://doi.org/10.1049/mnl.2018.5825

[22] Sinha G, Adhikary K, Chaudhuri S (2005) Sol-gel derived phase pure α-$Ga_2O_3$ nanocrystalline thin film and its optical properties. J Cryst Growth 276:204–207. https://doi.org/10.1016/j.jcrysgro.2004.11.375

[23] Zhu Y et al (2021) Growth and nitridation of β-$Ga_2O_3$ thin films by sol-gel spin-coating epitaxy with post-annealing process. J Sol-Gel Sci Technol 100: 183–191. https://doi.org/10.1007/s10971-021-05629-4

[24] Gopal R et al (2018) Sol- gel synthesis of $Ga_2O_3$ nanorods and effect of precursor chemistry on their structural and morphological properties. Ceram Int 44:19099–19105. https://doi.org/10.1016/j.ceramint.2018.07.173

[25] Minami T, Shirai T, Nakatani T, Miyata T (2000) Electroluminescent devices with Ga2O3: Mn thin-film emitting layer prepared by sol-gel process. Jpn J Appl Phys 39:L524–L526. https://doi.org/10.1143/jjap.39.l524

[26] Liu Q et al (2018) Stabilizing the metastable γ phase in $Ga_2O_3$ thin films by Cu doping. J Alloys Compd

731:1225–1229. https://doi.org/10.1016/j.jallcom.2017.10.162

[27] Li Y, Trinchi A, Wlodarski W et al (2003) Investigation of the oxygen gas sensing performance of $Ga_2O_3$ thin films with different dopants. Sens Actuators B Chem 93:431–434. https://doi.org/10.1016/S0925-4005(03)00171-0

[28] Kokubun Y, Nakagomi AT, S, (2010) Sol–gel prepared $(Ga_{1-x}In_x)_2O_3$ thin films for solar-blind ultraviolet photodetectors. Physica Status Solidi (a) 207:1741–1745. https://doi.org/10.1002/pssa.200983712

[29] Shen H, Yin Y, Tian K et al (2018) Growth and characterization of β-$Ga_2O_3$ thin films by sol-gel method for fast-response solar-blind ultraviolet photodetectors. J Alloys Compd 766:601. https://doi.org/10.1016/j.jallcom.2018.06.313

[30] Yu M, Lv C, Yu J et al (2020) High-performance photodetector based on sol-gel epitaxially grown α/β$Ga_2O_3$ thin films. Mater Today Commun 25:101532. https://doi.org/10.1016/j.mtcomm.2020.101532

[31] Kokubun Y, Miura K, Endo F, Nakagomi S (2007) Sol-gel prepared β-$Ga_2O_3$ thin films for ultraviolet photodetectors. Appl Phys Lett 90:031912. https://doi.org/10.1063/1.2432946

[32] Fan M, Cao L, Xu K, Li X (2021) Mixed-phase β-$Ga_2O_3$ and $SnO_2$ metal-semiconductor -metal photodetectors with extended detection range from 293 nm to 330 nm. J Alloys Compd 853:157080. https://doi.org/10.1016/j.jallcom.2020.157080

[33] Mukhopadhyay P, Schoenfeld WV (2019) Tin gallium oxide solar-blind photodetectors on sapphire grown by molecular beam epitaxy. Appl Opt 58:D22-27. https://doi.org/10.1364/AO.58.000D22

[34] Zhao X, Cui W, Wu Z et al (2017) Growth and characterization of Sn doped β-$Ga_2O_3$ thin films and enhanced performance in a solar-blind photodetector. J Electron Mater 46:2366. https://doi.org/10.1007/s11664-017-5291-5

[35] Du X, Li Z, Luan C et al (2015) Preparation and characterization of Sn-doped β-$Ga_2O_3$ homoepitaxial films by MOCVD. J Mater Sci 50:3252–3257. https://doi.org/10.1007/s10853-015-8893-4

[36] Fan M, Lu Y, Xu K, Cui Y, Cao L, Li X (2020) Growth and characterization of Sn-doped β-$Ga_2O_3$ thin films by chemical vapor deposition using solid powder precursors toward solar-blind ultraviolet photodetection. Appl Surf Sci 509:144867. https://doi.org/10.1016/j.apsusc.2019.144867

[37] O'Donoghue R, Rechmann J, Aghaee M et al (2017) Low temperature growth of gallium oxide thin films via plasma enhanced atomic layer deposition. Dalton Trans 46:16551–16561. https://doi.org/10.1039/c7dt03427j

[38] Tao J, Lu H, Gu Y et al (2019) Investigation of growth characteristics, compositions, and properties of atomic layer deposited amorphous Zn-doped $Ga_2O_3$ films. Appl Surf Sci 476:733–740. https://doi.org/10.1016/j.apsusc.2019.01.177

[39] Guo D, Liu H, Li P et al (2017) Zero-power-consumption solar-blind photodetector based onβ-$Ga_2O_3$/NSTO heterojunction. ACS Appl Mater Interfaces 9:1619–1628. https://doi.org/10.1021/acsami.6b13771

[40] Liao Y, Jiao S, Li S et al (2018) Effect of deposition pressure on the structural and optical properties of $Ga_2O_3$ films obtained by thermal post-crystallization. Cryst Eng Comm 20:133–139. https://doi.org/10.1039/c7ce01567d

[41] Batzill M, Diebold U (2005) The surface and materials science of tin oxide. Prog Surf Sci 79:47–154. https://doi.org/10.1016/j.progsurf.2005.09.002

[42] Zhao J, Sun X, Ryu H, Tan ST (2011) UV and visible electroluminescence from a Sn:$Ga_2O_3$/$n^+$-Si heterojunction by metal-organic chemical vapor deposition. IEEE T Electron Dev 58:1447–1451. https://doi.org/10.1109/ted.2011.2112364

[43] Nakagomi S, Kokubun Y (2012) Crystal orientation of β-$Ga_2O_3$ thin films formed on c-plane and a-plane sapphire substrate. J Cryst Growth 349:12–18. https://doi.org/10.1016/j.jcrysgro.2012.04.006

[44] Zhang M, Xu M, Li M et al (2017) $SnO_2$ epitaxial films with varying thickness on c-sapphire: structure evolution and optical band gap modulation. Appl Surf Sci 423:611–618. https://doi.org/10.1016/j.apsusc.2017.06.250

[45] Kumar SS, Rubio EJ, Noor-A-Alam M et al (2013) Structure, morphology, and optical properties of amorphous and nanocrystalline gallium oxide thin films. The J Phys Chem C 117:4194–4200. https://doi.org/10.1021/jp311300e

[46] Manandhar S, Ramana CV (2017) Direct, functional relationship between structural and optical properties in titanium-incorporated gallium oxide nanocrystalline thin films. Appl Phys Lett 110:061902. https://doi.org/10.1063/1.4974042

[47] Manandhar S, Battu AK, Tan S, Panat R, Shutthanandan V, Ramana CV (2019) Effect of Ti doping on the crystallography, phase, surface/interface structure and optical band gap of $Ga_2O_3$ thin films. J Mater Sci 54:11526–11537. https://doi.org/10.1007/s10853-019-03663-w

[48] Dakhel AA (2012) Structural, optical, and opto-dielectric properties of W-doped $Ga_2O_3$ thin films. J Mater Sci 47:3034–3039. https://doi.org/10.1007/s10853-011-6134-z

[49] Guo D, Qin X et al (2017) Decrease of oxygen Vacancy by Zn-doped for improving solar-blind photoelectric performance in β-$Ga_2O_3$ thin films. Electron Mater Lett 13:483–488. https://doi.org/10.1007/s13391-017-7072-y

[50] Guo X, Hao N, Guo D et al (2016) β-$Ga_2O_3$/p-Si heterojunction solar-blind ultraviolet photodetector with enhanced photoelectric responsivity. J Alloys Compd 660:136–140. https://doi.org/10.1016/j.jallcom.2015.11.145
[51] Fan M, Liu K, Chen X et al (2015) Mechanism of excellent photoelectric characteristics in mixed-phase ZnMgO ultraviolet photodetectors with single cutoff wavelength. ACS Appl Mater Interfaces 7:20600–20606. https://doi.org/10.1021/acsami.5b04671
[52] Jiang D, Tian C, Yang G et al (2015) $Mg_xZn_{1-x}O$ solar-blind photodetectors fabricated by RF magnetron sputtering with combinatorial targets. Mater Res Bull 67:158–161. https://doi.org/10.1016/j.materresbull.2015.03.025
[53] Lin R, Zheng W, Zhang D et al (2018) High-performance graphene/β-$Ga_2O_3$ heterojunction deep-ultraviolet photodetector with hot-electron excited carrier multiplication. ACS Appl Mater Interfaces 10:22419. https://doi.org/10.1021/acsami.8b05336

**Publisher's Note** Springer Nature remains neutral with regard to jurisdictional claims in published maps and institutional affiliations.